

Check for updates

www.am-journal.

Crafting Tunable Hollow Particles Using Antisolvent-Driven Interlocking of Micron-Sized Building Blocks

Peilong Li, Jieying Li, Jacob Levin, Arkaye Kierulf, James Smoot, Amin Zarei, and Alireza Abbaspourrad*

The contribution of a hollow structure on the rheological behavior of granular suspensions remains un-investigated due to the challenge of water impermeability. Here starch is used to fabricate water-permeable hollow particles, as a model for granular suspensions and investigated the resulting microstructures and rheological behavior. The hollow structure is fabricated based on a bottom-up method by assembling micron-sized building blocks into a superstructure. A Pickering emulsion is heated to fuse the starch interface, then, upon antisolvent precipitation, the polymer strands interlock to form a rigid shell around the oil template. When the template is removed a hollow particle remained. These particles exhibited a specific volume >5-times higher than unmodified starch and consequently a higher viscosity. Larger particles showed higher viscosity but are also more fragile. The template structure can be manipulated to fine-tune their functionality. These micro-sized building blocks made from edible materials can be used as the next generation of texturizers. Additionally, these water-permeable colloidosomes present an innovative approach to understanding how micro-architectures impact the rheological behavior of granular suspensions.

1. Introduction

Granular suspensions, non-Brownian particles suspended in fluid media, are ubiquitous from concrete slurry used in construction to peanut butter. Understanding the rheological behavior of these particle suspensions is crucial to uncovering, refining, and using the mechanical properties of these materials. A fundamental aspect of rheological measurement is to gain insight into the microstructure of material underflow.

The viscosity of a granular suspension increases with a higher volume fraction of particles, that is, more particles impede the fluid flow. The increase of viscosity is linear in a diluted system

P. Li, J. Li, J. Levin, A. Zarei, A. Abbaspourrad
Department of Food Science
Cornell University
Ithaca, NY 14853, USA
E-mail: alireza@cornell.edu
A. Kierulf, J. Smoot

Tate & Lyle Solutions USA LLC 5450 Prairie Stone Pkwy, Hoffman Estates, IL 60192, USA

The ORCID identification number(s) for the author(s) of this article can be found under https://doi.org/10.1002/adfm.202313025

DOI: 10.1002/adfm.202313025

because flow further from the particles remains unaffected.[1] In a more concentrated system, the hydrodynamic interactions between the particles become stronger, which in turn changes the rate of energy dissipation.^[2] The linear function of viscosity is then distorted in the presence of higher fractions.[3] As the volume fraction approaches the maximum packing fraction, the viscosity increases sharply due to the stronger interference within the narrowed interstitial space.[4] The dense granular suspension forms a solid-like material, which is attributed to the jamming transition where particles and fluid are immobilized. The dynamic arrest and jamming phenomenon that results from high volume fractions are used to create structures that have wide applicability across industries, from silicon particles in robotic grippers to air bubbles in whipped cream. [5-8] To modulate the mechanical properties, the packing behavior has been investigated by manipulating particle morphology such as

polydispersity and shape, and the amount of materials required for dense packing can be altered by a volume fraction of ≈ 0.1 . [9-11]

Besides the external characteristics of the particles, another factor that has been largely overlooked, hollowness, can affect the amount of material needed for dense packing. For instance, a hollow sphere with a 100- μ m diameter with a 1- μ m wall requires only 6 w/w% solid compared to a non-hollow particle of the same volume and material; thus, a hollow sphere would require much less material to reach the same packing fraction. Consequently, at limited solid content, the suspension with hollow particles with easier jamming and a higher volume fraction is expected to contribute to an altered rheological behavior through more effective hydrodynamic interactions.

Despite hollow particles having demonstrated extraordinary ability with respect to thermal resistance, [12] drug delivery, [13,14] and microreactors, [15] the impact of hollow structures on rheological behavior has not been explored. We speculate this is because the hollow particles reported by previous studies, such as glass beads, [16] plastic particles, [17] and even microorganisms, [18] are impermeable to water and float as a separate phase that is not incorporated into the suspension. Thus, to understand the contribution that hollow structures make on rheological behavior, fabrication of water-permeable particles is required as hydration of the core reduces the difference in density between the particles

1616328, 0, Downloaded from https://onlinelibrary.wiley.com/doi/10.1002/adfm.202313025 by Cornell University Library, Wiley Online Library on [1.042024]. See the Terms and Conditions (https://onlinelibrary.wiley.com/terms-and-conditions) on Wiley Online Library for rules of use; OA archies are governed by the applicable Creative Commons Licenses

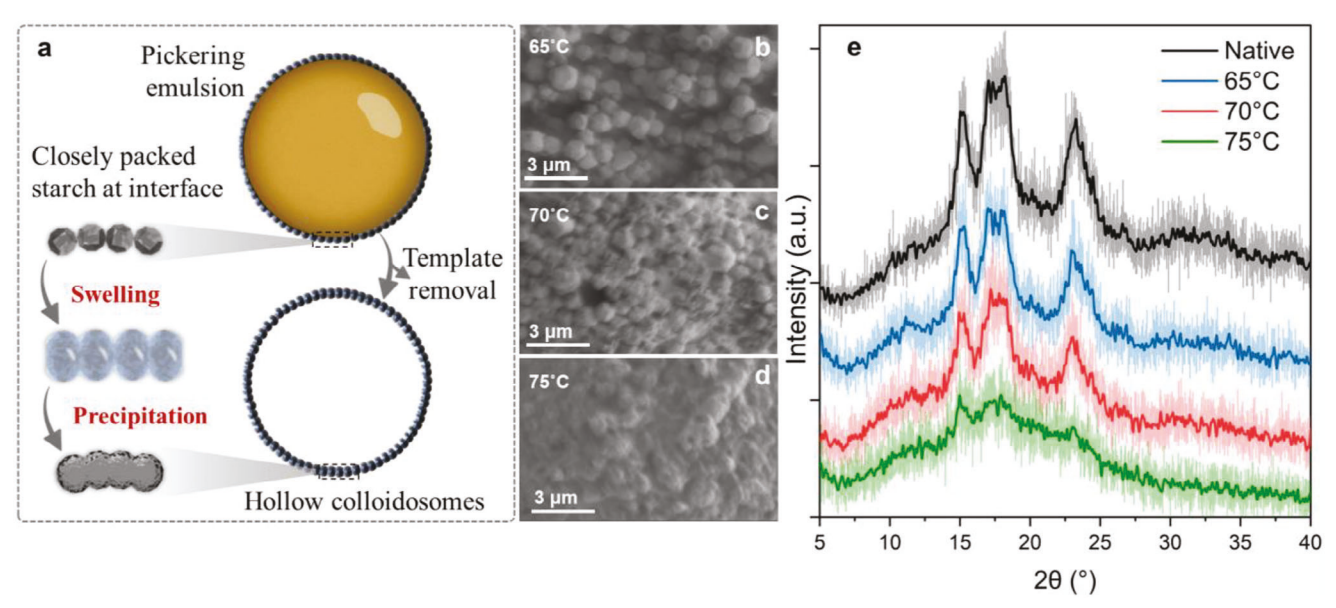


Figure 1. a) Schematic diagram of bottom-up method templated on Pickering emulsion to fabricate starch hollow particles. b–d) Scanning electron microscopy (SEM) photos of amaranth starch incubated at 65, 70, and 75 °C. e) X-ray diffreaction (XRD) patterns of starch heated at different temperatures

and the continuous fluid phase thus forming an analyzable granular suspension. With water trapped in the hollow particles, the amount of fluid in the continuous phase can be reduced while maintaining the same solid content that would result in an increase in granular volume fraction. This increase is expected to alter rheological behavior by allowing stronger hydrodynamic interactions.

Here, we used starch, a carbohydrate biopolymer, as the material to fabricate water-permeable hollow particles which can be used as a model to investigate the effect of hollow structures on rheological behavior. We hypothesized that water is able to diffuse into the core when the starch polymer becomes hydrated, and the suspension of hollow granules will exhibit a high-volume fraction given a limited amount of solid and alter the rheological behavior of the suspension.

In its natural state, starch is composed of rigid particles with different granular sizes from 1 to 100 µm depending on its botanical source. [19] Although starch modification has been studied for over a century, none of the conventional modification methods have produced particles with a hollow structure. [20] We present a novel bottom-up approach for the production of hollow starch particles. Our proposed method involves assembling small starch building blocks into a colloidosome superstructure, that is, an assembly of particles that have an empty internal cavity and are densely packed on the surface. [21,22]

The architecture of colloidosomes has diverse applications, such as cargos for drug delivery, [13] enzyme micro-reactors, [15] tailored micro-swimmers, [23] or protocells for bio-signaling. [24] One of the most commonly used methods for preparing colloidosomes is based on Pickering emulsions, where droplets are stabilized by insoluble particles. [25] Because the particles are wettable by both water and oil, they remain at the interface at a certain angle immersed in both phases, and form a layer around the curvature of the droplet. [26] Through physical fusion or chemical

bonding, the Pickering particles became integrated into a shell, and subsequently, a colloidosome formed.^[25]

Starch is a biodegradable and food-safe material used to stabilize Pickering emulsions.^[27] Amaranth starch, the smallest granular dimension found in nature (1 µm),[28] as a Pickering emulsifier is able to produce droplets on the scale of tens of microns, which can be used as the building blocks for constructing hollow superstructures.^[29] We postulate that heating starch-coated oil droplets in water will dissociate the hydrogen bonds in the crystalline region and the granules will swell, forcing neighboring particles to fuse and form an integrated layer around the oil phase (Figure 1a).[30,31] Subsequent dehydration, using an antisolvent, of the interface would trigger the starch strands to interlock and form a rigid starch shell around the oil. Once the oil phase is removed a stable hollow colloidosome structure composed of tangled starch molecules would remain. The resulting thermally activated carbohydrate polymer would be water-permeable, and its structured colloidosomes can be studied to advance our understanding of the effect of microstructure on rheological behavior. By creating hollow structures composed of multiple fused starch granules the thickening ability of the starch would be enhanced and reduce the amount of starch required to obtain the same viscosity.[28] Thus the development of super-thickeners based on the hollow-particle approach would allow food producers to reduce the starch content and as a result reduce calories, without compromising desirable organoleptic properties.[32-34]

2. Results and Discussion

2.1. Bottom-Up Assembly of Hollow Starch Particles

Raw amaranth starch are rigid solid particles with a granular size of $\approx 1~\mu m$ (Figure 1b). Native starch exhibits an A-type semicrystalline structure with the crystalline signal appearing at

16163028, 0, Downloaded from https://onlinelibrary.wiley.com/doi/10.1002/adfm.202313025 by Cornell University Library, Wiley Online Library on [11/04/2024]. See the Terms and Conditions (https://onlinelibrary.wiley.com/erms

and-conditions) on Wiley Online Library for rules of use; OA articles are governed by the applicable Creative Commons License

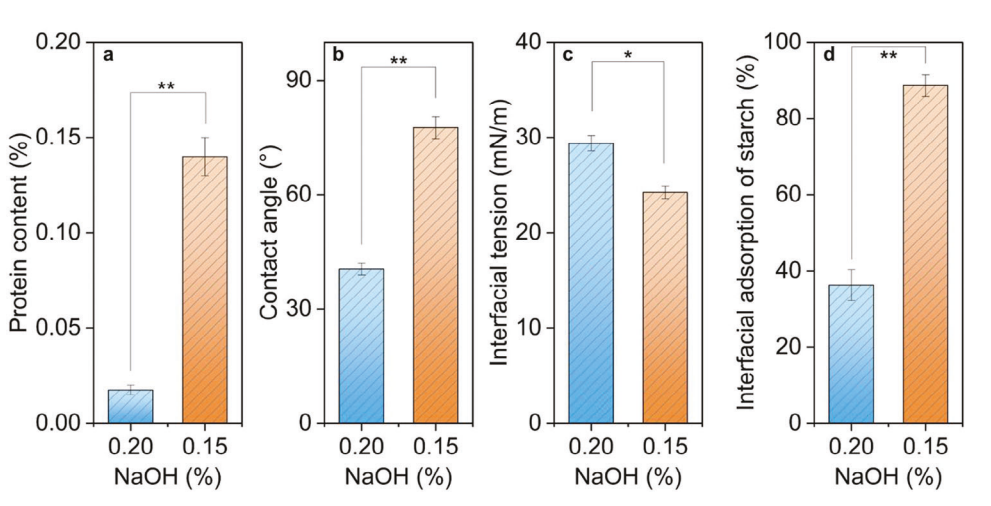


Figure 2. NaOH concentration during extraction affects starch a) protein content, b) contact angle, c) water-heptane interfacial tension, and d) interfacial adsorption of Pickering particles. Statistical significance is indicated by an asterisk (*p < 0.5, **p < 0.1).

15.2°, 17.5°, and 23.2° in the XRD (Figure 1e) due to the amylose and amylopectin polymers that are packed in a helix.[35,36] The gelatinization onset temperature for amaranth starch has been reported at 68 °C.[37] Above this temperature, the starch polymeric strands dissociate and the crystalline region melts (Figure 1e). When heated, the polymer chains, liberated from the double helices, exhibit higher conformational freedom allowing them to tangle and stick together with neighboring granules (Figure 1c,d). As a result, thermal treatment allows small starch granules to be incorporated into a superstructure.

Amaranth starch is the smallest naturally occurring starch suitable for use in a bottom-up template. To extract starch from amaranth flour, different alkaline concentrations were used (Figure 2). Higher alkaline concentrations (0.20 w/v% NaOH) removed most of the proteins from the raw material by increasing the negative charge on the proteins and increasing their solubility (Figure 2a). A lower NaOH concentration (0.15 w/v%) had higher protein retention (0.14 w/w% of starch), which in turn helped to enhance amphiphilicity. The high-protein starch shows a >75° water contact angle and stronger hydrophobicity compared to the low-protein starch (<45°) (Figure 2b). The high-protein starch was able to lower the water-heptane interfacial tension indicating the feasibility for emulsification (Figure 2c).

Upon emulsion formation, the amount of starch adsorbed onto the heptane-water interface was quantified (Figure 2d). When the protein content was too low, the majority of starch particles were found in a free non-adsorbed form, thus they were not suitable for constructing a template. In contrast, with higher protein content ≈90% of the starch particles migrated to the droplet surface. High-protein starch was found to develop a bulky template and the starch materials used for the rest of our study were all extracted by 0.15 w/v% NaOH.

The hollow particles are formed in four distinct steps: Pickering emulsion formation, fusion of the starch shell, antisolvent precipitation of the shell, and removal of the organic template to produce the hollow particle (Figure 3). To begin, small starch granules (1 µm) are closely packed around the interface of oil droplets within an aqueous phase forming a Pickering emulsion. This interface is observed as an opaque surface around the

droplet as observed using optical microscopy (Figure 3a). Once the emulsion is formed, heat treatment allows the crystalline region of the starch particles on the interface to dissociate and tangle with neighboring particles, this also allows water to seep into the softened granules. Visually this change is marked by the dark interface becoming transparent (Figure 3b).

Following hydrothermal treatment, the hydrated granules were expected to have higher water wettability, indicated by a lower contact angle and lower desorption energy (E). However, desorption energy increases with increasing particle size, (E = $\pi R^2 \gamma (1 - \cos\theta)^2$, where R is the radius of the interfacial particle and θ is the contact angle); therefore, when the starch swells, the reduction in E originally attributed to the starch's higher wettability is negated, thus the particles remain at the interface.^[38] The starch-stabilized emulsions are thermally stable and show no evidence of major droplet coalescence or catastrophic phase separation, which is attributed to the non-desorbed Pickering particles. The swollen granules form a gel barrier consistent with a previous study where a thickened starch layer reduced the uncovered pores between interfacial Pickering particles.^[39]

Ethanol is both an antisolvent to starch and a miscible cosolvent with water. As a result, when ethanol is added to the gelatinized starch emulsions, the starch particles at the interface lose their affinity for water and precipitate. This leads to the extraction of water from the starch layer, which shrinks the interface and forces the particles to interlock and form a shell. To purify the precipitated shell, additional ethanol is used to remove residual water. The shell needs to be dehydrated; otherwise, the organic solvent cannot penetrate which would impede the removal of the internal organic template. Upon removal of water, the droplet surface becomes dark again as the interface shrinks and forms an opaque interlocked solid shell (Figure 3c). The dynamic process of antisolvent precipitation is rapid, < 2 s (Movie \$1, Supporting

Precipitated and dehydrated shells were then washed with hexane to remove the organic phase, including the heptane in the core and residual ethanol in the continuous phase. During this process the particles become transparent (Figure 3d). Once the template organic phase is removed the starch maintains the

1616328, 0, Downloaded from https://onlinelibrary.wiley.com/doi/10.1002/adfm.202313025 by Cornell University Library, Wiley Online Library on [1.042024]. See the Terms and Conditions (https://onlinelibrary.wiley.com/terms-and-conditions) on Wiley Online Library for rules of use; OA archies are governed by the applicable Creative Commons Licenses

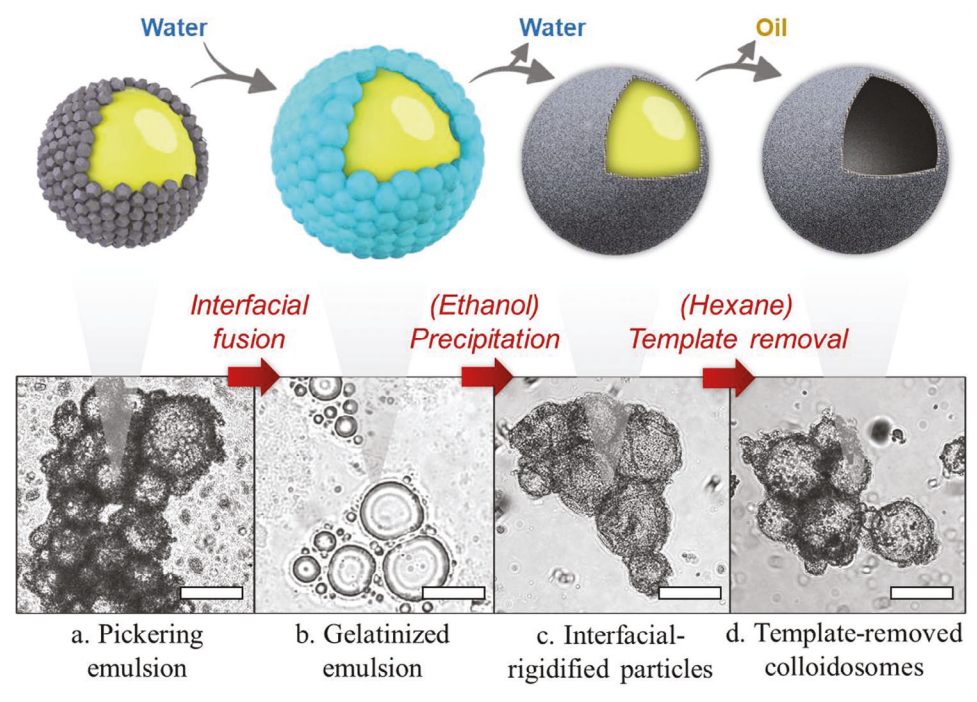


Figure 3. Optical microscopic photos of droplets/particles at different fabrication stages: a) Pickering emulsion, b) gelatinized emulsion, c) particles with ethanol-precipitated interface, d) hexane-washed hollow particles. The emulsion was prepared with 30 w/w% heptane and 3 w/w% amaranth starch at the homogenizer speed of 20,000 rpm. The scale bars are 100 µm.

assembled spherical superstructure. This suggests that the structural properties of the colloidosomes are the result of their unique volume expansion after heating and the intermolecular forces that are present between them upon solvent exchange.

Thermal-induced fusion is a critical stage in the fabrication process. Without heating, when the interior heptane was removed, we observed a collapse of the structure. This is because the starch particles on the surface did not contact enough with their neighboring particles, and the curvature of a droplet relies on the Laplace pressure between the water-oil interface.^[40] Thermal treatment integrates the discrete particles into a gelatinized whole, and then the structure is not dependent on the wateroil interface but rather the polymer entanglements which convert the emulsion template into a colloidosome. However, when the emulsion is heated for an extended period at high temperature, the colloidosomes collapse because amylose leaches from the starch granules during prolonged gelatinization, causing the shell to lose its granular integrity and not interlock well (Figure \$1, Supporting Information).[41]

Another critical step of successful structuring is solvent evaporation. We found that even after the solid starch interface had been precipitated, evaporating the ethanol without adding hexane, led to the structural collapse of the colloidosome (Figure S2a,b, Supporting Information). However, washing away ethanol with hexane before solvent evaporation was found to be effective in retaining the structure after complete solvent evaporation (Figure S2c,d, Supporting Information). One possible reason for this phenomenon is that although ethanol is an antisolvent for starch, it can still interact with starch molecules through hydrogen bonds, [42] thus when ethanol is evaporated it could rupture the tangled starch strands causing the structure to collapse. Using hexane as a solvent in the last step allows the hollow particles to remove both residual ethanol and heptane.

The starch colloidosomes were analyzed by Fourier-transform infrared spectroscopy (FTIR) to ensure the removal of hexane. The adsorption bands corresponding to the -OH group of the starch at 3321 cm⁻¹ and the -CH group at 2926 cm⁻¹ of the starch samples were used to determine if hexane remained (Figure 4a). The starch colloidosomes, suspended in hexane, showed bands at 3321 and 2926 cm^{-1} , and the ratio of intensity was 0.94(Figure 4b). After drying, the value increased to 1.96, similar to unmodified starch (p > 0.05), suggesting that all of the hexane had been removed. In addition, the dried starch was analyzed using solid-state ¹³C NMR, where all carbons observed were from carbohydrates and no peaks for hexane were observed (Figure 4c). The ability to completely remove all organic solvents used, as well as the organic phase, makes these starch colloidosomes suitable for use in food.

After the hexane is evaporated, starch particles with a hollow structure remain (Figure 5a). When the same mass of hollow particles is compared to unmodified starch particles, the volume of the hollow particles is much larger due to their open internal compartment (Figure 5b). When hollow starch particles were redispersed in water, initially a solid layer floated on the surface of the liquid due to the low density of hollow particles (0.1 g mL⁻¹) (Figure 5c). During the thermal processing step, the hydroxyl groups on the starch chains become exposed and they facilitate water diffusion into the interior of the starch cage. As a result, the water-permeated starch eventually settles to the bottom and the bubble rings present in the dried samples disappear, but the starch shells still maintain their superstructure (Figure 5d). The fabrication of these water-permeable hollow starch particles

16163028, 0, Downloaded from https://onlinelibrary.wiley.com/doi/10.1002/adfm.202313025 by Cornell University Library, Wiley Online Library on [11/04/2024]. See the Terms and Conditions (https://onlinelibrary.wiley.com/

conditions) on Wiley Online Library for rules of use; OA articles are governed by the applicable Creative Commons License

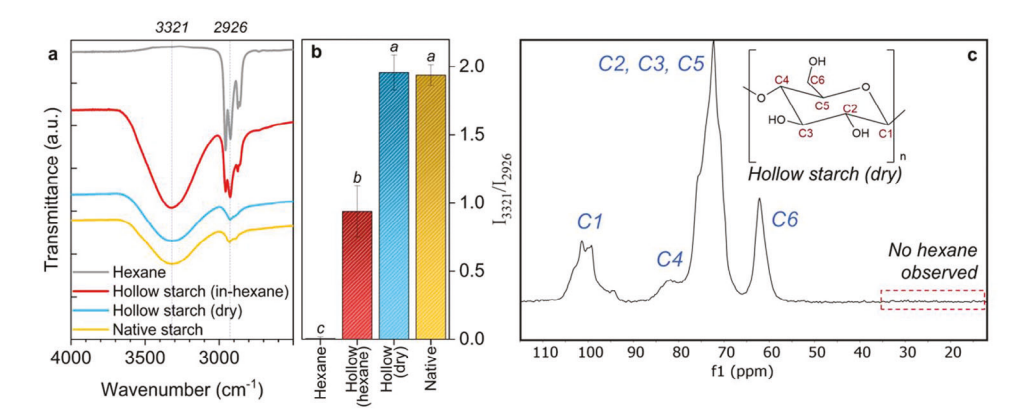


Figure 4. a) FTIR spectra of hexane (grey), hollow-starch suspension in hexane (red), dry hollow particles (blue), and native starch (yellow). b) The intensity ratio of the peak at 3321 cm⁻¹ and 2926 cm⁻¹. Different letters indicate statistical difference p < 0.05. (c) ¹³C solid-state NMR spectrum of dry hollow starch, no hexane peaks were observed between 12 and 32 ppm.

provided a practical platform to study the effect of hollow structures on rheological behavior.

2.2. Manipulation of Emulsification Process to Tune Properties of Starch Colloidosome

The conditions of emulsification, such as homogenizer shear speed, play a crucial role in determining the properties of the resulting starch cage; it affects the size and distribution of the primary oil droplets. To probe this, emulsions were prepared us-

ing different homogenizer speeds and used to make different samples of colloidosomes and these particles were evaluated for porosimetry, rheometry, and morphology.

The mercury porosimetry was scanned from 0.3 to $30\,000$ psia with the corresponding pore size ranging from 0.005 to $300\,\mu m$ (Figure 6a). The magnitude of pressure exerted is indicative of pore size, where low pressure corresponds to larger pores, and high pressure corresponds to smaller pores based on the Washburn equation. For native starch, the total intrusion volume was only $0.77\, \text{mL g}^{-1}$ indicating a limited porosity and higher density (Table S1, Supporting Information). Conversely, the

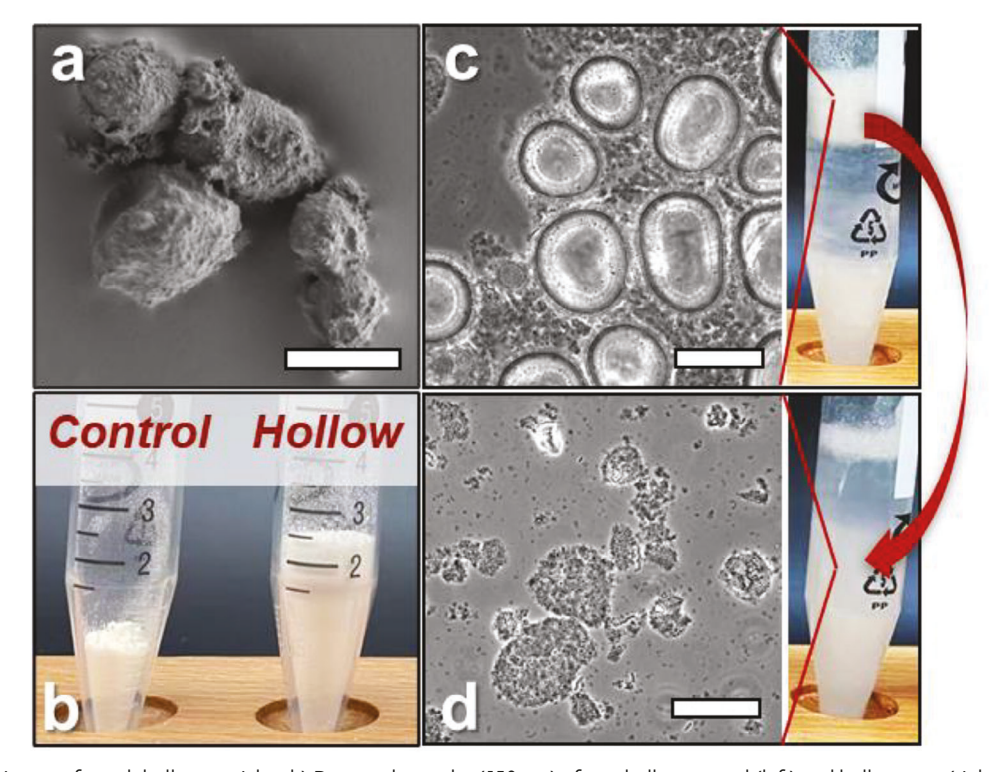


Figure 5. a) SEM image of starch hollow particles. b) Dry starch powder (150 mg) of non-hollow control (left) and hollow cage (right). c) Air cells formed when hollow starch is added to water. d) Water diffused into the starch cage. The scale bars are $100 \mu m$.

16163028, 0, Downloaded from https://onlinelibrary.wiley.com/doi/10.1002/adfm.202313025 by Cornell University Library, Wiley Online Library on [11/04/2024]. See the Terms and Conditions (https://onlinelibrary.wiley.com/term

and-conditions) on Wiley Online Library for rules of use; OA articles are governed by the applicable Creative Commons I

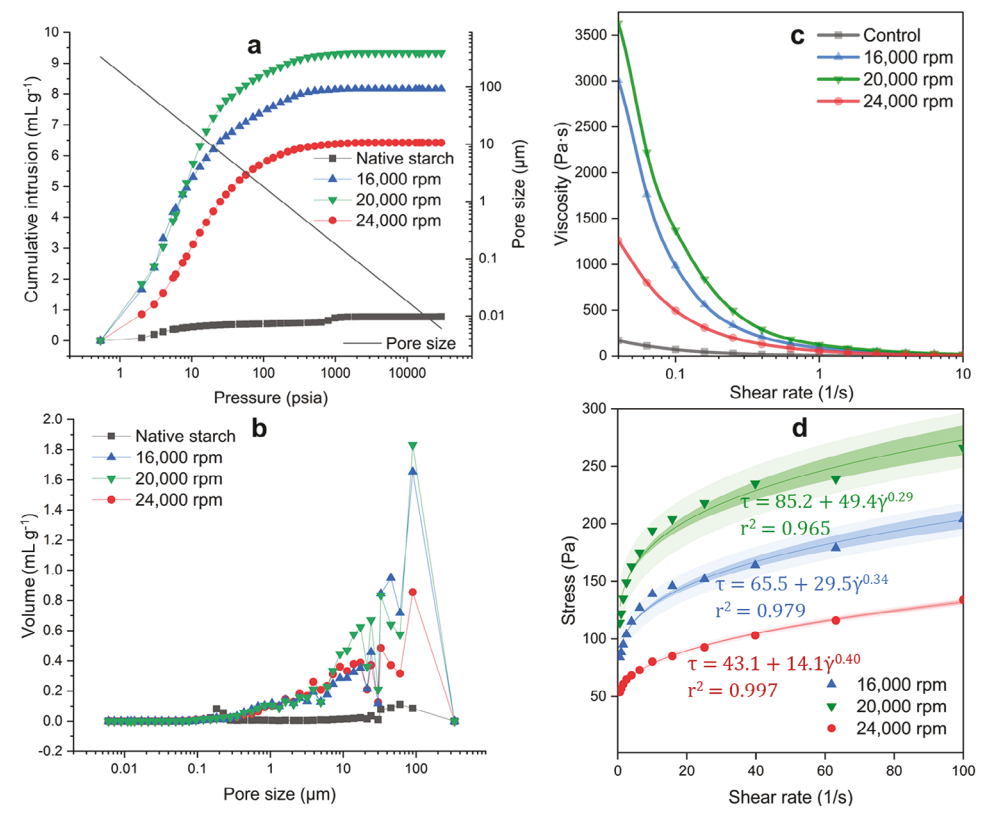


Figure 6. Emulsification shear speed (16 000, 20 000, 24 000 rpm) affected hollow particles on microstructure and rheological properties: a) cumulative intrusion volume of mercury at different pressures, b) volume distribution of pore size, c) viscosity of slurry (13 w/w%), d) shear stress fitted to Herschel–Bulkley model. The inner and outer bands of the regression curves represent 95% confidence intervals and 95% prediction intervals, respectively.

hollow starch particles produced from emulsions created with a homogenizer speed of 24 000 rpm showed that initially, as the pressure increased, the intrusion volume exhibited a sharp increase indicative of large pores at the low-pressure region (<100 psia). However, as the pressure continued to rise, the intrusion volume reached a plateau and remained constant. Overall, colloidosomes prepared with the homogenizer at 24 000 rpm were able to trap over 6 mL of mercury per gram of porous particles, which was ≈8-fold higher compared to the unmodified starch. The porosity increased from 52% for native amaranth starch to 86% for the hollow particles prepared from 24 000 rpm homogenization, and the bulk density decreased from 0.67 to 0.13 g mL⁻¹ (Table S1, Supporting Information). This sharp change is due to the assembly of small amaranth starch particles into a superstructure thus providing higher volume via the empty internal compartment for the same solid mass. The volume distribution of pore size (Figure 6b) shows that mercury was pressed into native starch mainly through pores ≈200 nm which could be attributed to the nanochannels present in starch granules.[44] In contrast, the intrusion volume of the hollow starch particles is mainly attributed to the voids populated above the micron-scale dimension (Figure 6b).

When the homogenizer shear speed for emulsification decreased from 24 000 to 20 000 rpm, we observed a further increase in intrusion volume to > 9 mL g $^{-1}$ starch (Figure 6a). The porosity increased to 88%, with respect to hollow particles prepared at 24 000 rpm, and the bulk density was reduced to below

 $0.09~{\rm g~mL^{-1}}$ (Table S1, Supporting Information). Higher intrusion volume, increased porosity, and a lower bulk density are consistent with a lower homogenizer shear speed producing bulkier cages. Further decreasing the shear speed to 16 000 rpm, however, lowered the intrusion volume compared to the samples prepared at 20 000 rpm indicating a lower porosity and higher density (Figure 6a).

Increasing the emulsification speed from 16 000 to 24 000 rpm, decreased the average droplet size from 115 to 69 μ m, and the most abundant population shifted from $\approx 50~\mu$ m at 24 000 rpm to $\approx 20~\mu$ m at 16 000 rpm (Figure 7a). A slower homogenizer shear speed led to a lower Weber number, the disruption effect to overcome surface energy, which resulted in the production of larger droplets; lower shear speeds do not provide enough stress to overcome surface tension and thus cannot break up the organic phase as efficiently which leads to larger oil droplets being dispersed in the aqueous phase. [45] Conversely, a faster homogenizer shear speed produces smaller droplets due to the higher shear forces being applied to the emulsion, which results in a more efficient breakup of the oil phase. [40]

Droplet size has a significant impact on the properties of the starch cage that forms around them: larger droplets are expected to form larger colloidosomes while smaller droplets are expected to produce smaller colloidosomes. However, based on the porosimetry results, particles fabricated at 16 000 rpm unexpectedly exhibited lower porosity (i.e., smaller hollow particles)

16163028, 0, Downloaded from https://onlinelibrary.wiley.com/doi/10.1002/adfm.202313025 by Cornell University Library, Wiley Online Library on [11/04/2024]. See the Terms

litions) on Wiley Online Library for rules of use; OA articles are governed by the applicable Creative Commons

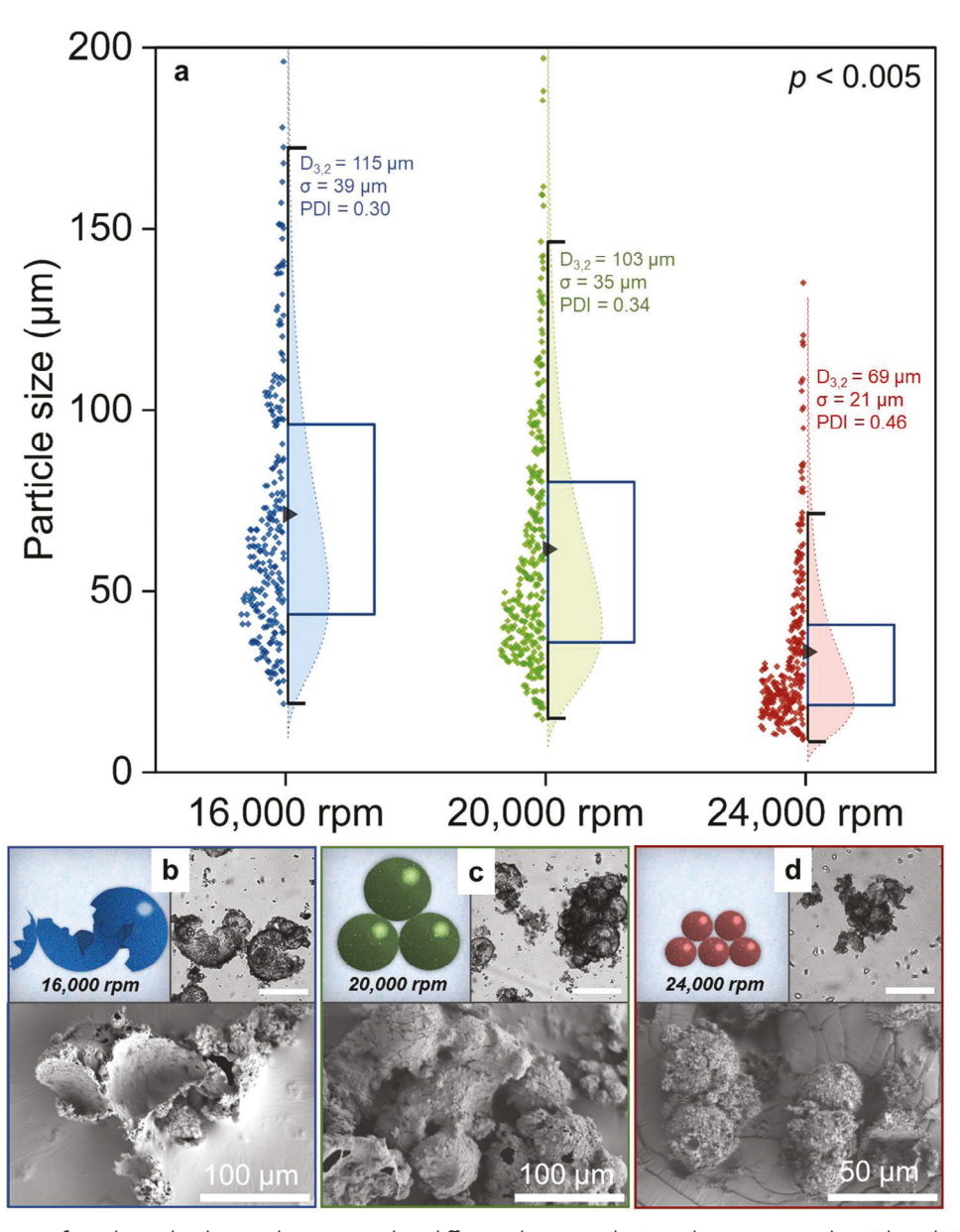


Figure 7. a) Distribution of emulsion droplet size homogenized at different shear speeds. Box plots represent the 25th and 75th percentiles with arithmetic means indicated in the middle. Sauter mean $(D_{3,2})$, standard deviation (σ) , and polydispersity index (PDI) of each population are noted. Each pair was tested using the nonparametric Wilcoxon method (p < 0.005). b–d) The optical microscopic photos and SEM images of hollow starch particles prepared from Pickering emulsion homogenized at 16 000, 20 000, and 24 000 rpm, respectively. The scale bars are 100 μm if not specified.

than those prepared at 20 000 rpm (Figure 6a). A possible reason is that when droplets become too large they cannot maintain their shape upon dehydration: in the samples from the droplets homogenized at 16 000 rpm we observed a considerable amount of large broken cages, and these fractured shells altered the packing behavior reducing the porosity (Figure 7b). [46] The fracturing probably occurred when the emulsion was added to ethanol. When the starch-stabilized emulsion was thermally activated, water was absorbed into the interfacial layer. Then, when ethanol is added, it acts as both an antisolvent to starch and extracts water from the starch layer. Losing water shrinks the starch layer and solidifies on the oil surface. The starch layer has a micron-scale

thickness and can show a gradient of strain where the outer surface of the starch shrinks faster due to the higher concentration of ethanol compared to the inner part of the starch layer. This difference between the inner and outer surfaces of the starch layer can build up stress within the starch layer which causes fracturing. When higher shear speeds are used for emulsification, the droplets and cages that result are smaller and sturdier (Figure 7d). [47] We found the optimal homogenization shear rate to be 20 000 rpm where the structural integrity was robust while maintaining a higher specific volume (Figure 7c).

The viscosity of hollow-particle suspension was found to be over 10^3 Pa·s; however, the viscosity of the control (a suspension

1616328, 0, Downloaded from https://onlinelibrary.wiley.com/doi/10.1002/adfm.202313025 by Cornell University Library, Wiley Online Library on [1/042024]. See the Terms and Conditions (https://onlinelibrary.wiley.com/terms-and-conditions) on Wiley Online Library on [1/042024]. See the Terms and Conditions (https://onlinelibrary.wiley.com/terms-and-conditions) on Wiley Online Library for rules of use; OA articles are governed by the applicable Creative Commons Licenses

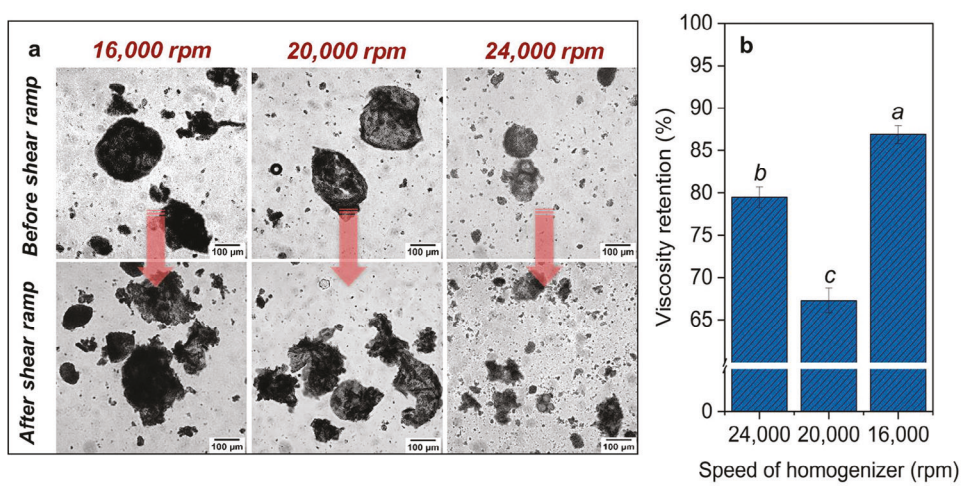


Figure 8. Mechanical stability of starch cages prepared from different homogenizer speeds (16 000, 20 000, and 24 000 rpm). a) Optical microscopic images of starch hollow particles before and after shear ramp $(0.01-100 \text{ s}^{-1})$. b) Viscosity retention after shear ramp $(0.01-100 \text{ s}^{-1})$. The letters above the error bar indicate a statistical difference (p < 0.5).

of non-hollow particles at the same solid content) was found to be much lower (Figure 6c). Superstructures formed by small particles with hollow interiors exhibit a higher volume fraction, especially when water in the continuous phase has been trapped inside the particles. When the water is trapped inside, there is less water in the continuous phase and consequently the particles are closer to each other. The force (*F*) required to squeeze the liquid at a certain velocity (v) through the gap between two particles (radius = r) increases with decreasing distance (h) $(F = \frac{1.5\pi\eta_0 vr^2}{r})$, which suggests that drag force is infinitely high when particles are in contact.^[2] The degree of improvement was found to be related to the speed of the homogenizer. Specifically, decreasing the homogenizer speed from 24 000 to 20 000 rpm resulted in higher viscosity due to the larger effective volume given the larger hollow structure of the colloidosomes prepared from droplets formed at 20 000 rpm.

The shear stress of starch slurry was plotted against the shear rate, and the results showed typical non-Bingham plastic properties, which were used to fit the Herschel-Bulkley model^[48] (Figure 6d). Hollow starch particles with large and intact cages exhibited higher yield stress (85.2 Pa) compared to others; however, the large intact hollow super-thickener showed stronger shearthinning behavior considering the low flow index (n = 0.29), which could be due to the rupture of hollow structures while being sheared.

Although high-shear homogenization is a scalable technique for industrial applications, an inherent limitation is that the templates produced are polydisperse (Figure 7a). Polydispersity may affect rheological behavior and mask the role of hollowness. To uncover the impact of polydispersity versus hollowness, we measured the viscosity of non-hollow potato starch (Figure S3, Supporting Information). Potato starch is a typical polydisperse system, [49] with a size span similar to the hollow starch fabricated from 24 000 rpm emulsification. The non-hollow polydisperse particles exhibited <10 Pa·s, which is lower than a typical monodisperse system. The viscosity of hollow particles, in contrast, is two orders of magnitude higher compared to the nonhollow polydisperse system. Therefore, although higher polydispersity reduces viscosity, the effect is minor compared to that enhanced by the bulky volume fraction contributed by hollow structures. However, future research should explore approaches to fabricate a perfectly monodisperse system, such as using microfluidic control.

The mechanical stability of the prepared cages was also studied to check if the hollow structure could survive after being sheared (Figure 8a). For the starch hollow particles prepared from 20 000 rpm, the large particles are intact before the shear, but after the shear ramp, a considerable number of the large particles were fractured. The mechanical sensitivity poses a challenge as the rheological study indicated that the viscosity retention was only 67% (Figure 8b; Figure S4, Supporting Information). The samples prepared at 24 000 rpm showed an increase in viscosity retention up to 80%, probably due to the smaller size of the hollow particles, which were less affected by mechanical stress and thus were able to preserve their integrity and functionality (Figure 8b; Figure S4, Supporting Information). The viscosity retention was 87% for starch particles prepared from 16 000 rpm, and this was attributed to the large number of starch cages that had already broken before the shear ramp, and therefore the viscosity was less sensitive to mechanical stress.

2.3. Template Composition Matters

The composition of a system can play a crucial role in emulsification, which may affect the formation of hollow particles upon the removal of the template. Emulsification is a complex process that involves the dispersion of an immiscible liquid phase, during this process, the amount of starch is an important factor, and the surface coverage is governed by the emulsifying agent which prevents coalescence of the dispersed droplets. Therefore, we evaluated the effect of the starch-to-oil ratio where an emulsion containing 30 w/w% heptane was produced using the same homogenization speed (24 000 rpm) and manipulated the ratio of raw materials (Figure 9). When more starch was used, the total

16163028, 0, Downloaded from https://onlinelibrary.wiley.com/doi/10.1002/adfm.202313025 by Cornell University Library, Wiley Online Library on [11/04/2024]. See the Terms and Conditions (https://onlinelibrary.wiley.com/erms

and-conditions) on Wiley Online Library for rules of use; OA articles are governed by the applicable Creative Commons License

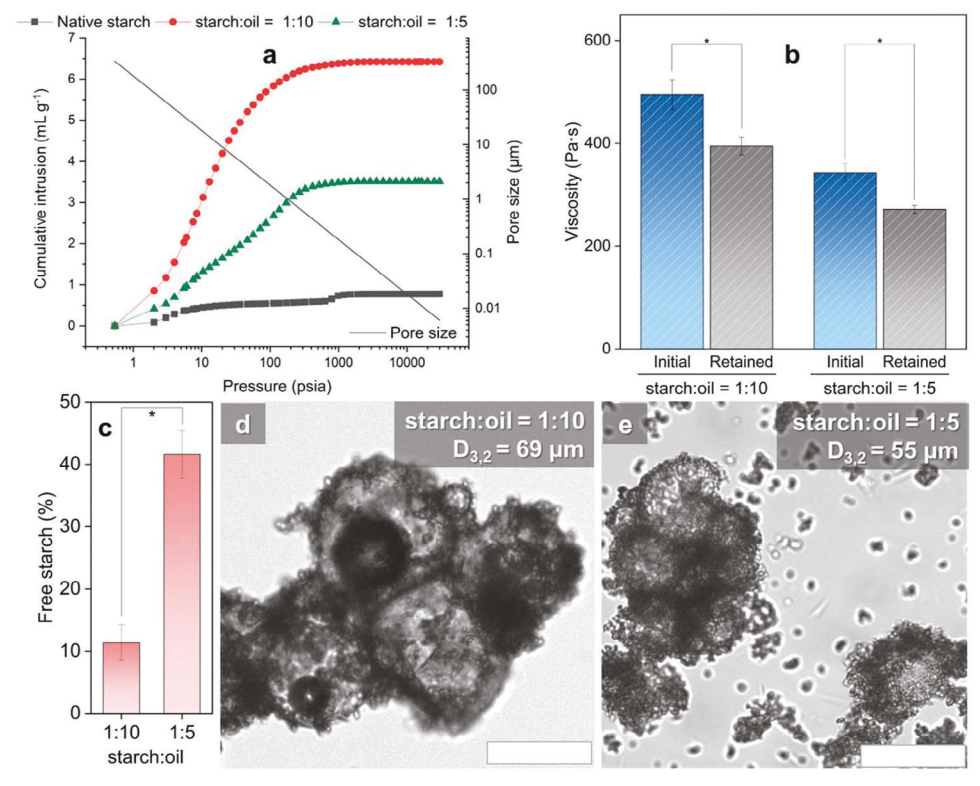


Figure 9. a) Starch-to-oil ratio of the emulsion template affects the structured volume of hollow particles. b) Initial and retained apparent viscosity ($\gamma = 0.1 \, \text{s}^{-1}$) of hollow particles fabricated from different starch-to-oil ratios. c–e) Free starch content and optical micrographs of the colloidosomes templates with different starch-to-oil ratios. Scale bar = 50 μ m. The emulsions contain the same oil fraction (30 w/w% heptane) and are emulsified at the same homogenizer speed (24 000 rpm). Statistical significance is indicated by an asterisk (*p < 0.5).

mercury intrusion decreased from 6.5 to 3.5 mL g⁻¹ (Figure 9a), and the porosity decreased from 86% to 77% with a higher bulk density (Table S2, Supporting Information). The pore size distribution indicates that when more starch is used for fabrication, smaller pores are produced (Figure S5a, Supporting Information). A lower viscosity was observed when starch content was doubled which could be due to a less effective volume (Figure 9b).

The reason for the low specific volume could be due to the smaller particle size that contributes to the more starch particles acting as emulsifiers (Figure 9d,e). The higher content of the emulsifier provides a more sufficient interfacial coverage and an enlarged surface area during emulsification, therefore producing smaller droplets. As a result, the volume-to-surface ratio decreases when the substrate has been removed. Another reason could be that when more starch is used as an emulsifier the surface becomes more saturated and an excess of non-adsorbed starch particles are dispersed in the aqueous phase (Figure 9c). As a result, the free individual particles cannot contribute to a high volume fraction as large bulky hollow particles, leading to a lower hydrodynamic interaction.

Emulsions with the same starch-to-oil ratio (1:10) were fabricated at the same homogenization shear speed (24 000 rpm), and the oil fraction was manipulated (Figure S6, Supporting Information). When more oil was emulsified as a template, the total mercury intrusion decreased from 6.5 to 2.6 mL g $^{-1}$, and the porosity decreased from 86% to 68% with a higher density. The distribution of pore sizes indicates that an increase in the amount of

organic phase used during emulsification resulted in the generation of a greater number of smaller pores (Figure S5b, Supporting Information). When higher oil fractions were used in the templating process, the resulting colloidosome group exhibited lower viscosity compared to those templated with lower oil fractions (Figure S6b, Supporting Information). This phenomenon is due to the increase in contact points between droplets in the higher internal phase of the emulsion, which leads to bridging between the neighboring droplets within the system (Figure S6c, Supporting Information). When the internal template used to create the hollow particles was removed, the resulting structure was a starch matrix rather than individual and intact colloidosomes (Figure S6d, Supporting Information). The bridged droplets are stabilized by a shared monolayer of starch.[51,52] The high oil fraction decreases the input of energy from emulsification which impedes the adoption of Pickering particles.^[53] Given a higher volume of dispersed phase with stronger bridging, the portion of non-adsorbed starch increased to over 30% and the free individual particles not contributing to a large hollow void resulted in a reduced volume fraction and thus lower viscosity (Figure S6e, Supporting Information). Stability against mechanical stress was also tested using two shear ramps, and the sample with a higher oil fraction showed weak shear stability with only 55% viscosity retention (Figure S6f, Supporting Information). The low viscosity retention observed in the group templated with a higher oil fraction can be attributed to the larger flocs which exhibit a lower debonding fracture energy.[54]

16162028, Downloaded from https://olinelibrary.wile.com/doi/10.1002/adfm.202313025 by Cornell University Library, Wiley Online Library on [1/10/40224]. Sethe Terms and Conditions (https://onlinelibrary.wiley.com/terms-and-conditions) on Wiley Online Library for rules of use; OA articles are governed by the applicable Creative Commons Licensed

3. Conclusion

Starch colloidosomes with hollow interiors were successfully prepared using a Pickering emulsion as a template where small individual starch particles assemble at the surface of an organic droplet. The assembled templates were then thermally activated to induce the fusion of interfacial particles, and the subsequent antisolvent precipitation triggered polymer interlocking and solidified the interface forming a rigid layer. When the internal oil phase was removed, hollow particles were produced. Emulsifying conditions, thermal activation, as well as solvent exchange, and evaporation, were identified as critical to avoid structural collapse. With a carbohydrate polymer as a shell, it allows water to seep into the hollow cores and these hollow, water-permeable particles serve as a platform to study the rheological behavior of hollow particles.

The produced starch colloidosomes exhibited larger specific volume and had a higher viscosity. The microstructure of hollow colloidosomes can be modulated by manipulating emulsification speed: mild homogenization helped to produce larger templates and thus larger hollow particles; however, if the emulsification shear speed is too low, hollow particles were less robust and ruptured during antisolvent precipitation. Template composition such as starch content and oil fraction also impacted the structure and functionality of the colloidosomes. Future research may explore approaches to improve the monodispersity and structural robustness of the colloidosomes to ensure their long-term stability and applicability.

Overall, water-permeable colloidosomes were successfully fabricated and used to demonstrate that the rheological behavior of a granular suspension can be modulated by tunable microarchitecture. With the food-safe carbohydrate polymers and the ease associated with their production, these hollow starch particles offer a scalable approach to serve as new texturizers with the potential to reduce carbohydrate content in future foods.

4. Experimental Section

Materials: Amaranth flour was purchased from Bob's Red Mill, Inc. (Milwaukie, OR, USA). Anhydrous ethanol (200 Proof) was purchased from Decon Labs, Inc. (King of Prussia, PA, USA). Sodium hydroxide, heptane, and hexane were purchased from Sigma-Aldrich (St. Louis, MO, USA).

Starch Extraction from Amaranth: Amaranth starch was extracted from amaranth flour using a previously published method (23, 24). Amaranth flour was steeped in a NaOH solution (0.15 or 0.20 w/v%) to extract starch. Insoluble fibers were sieved, and the liquid filtrate was centrifuged to separate the starch granules from the protein. The sediment was then neutralized, de-salted, and dried for further use.

Nitrogen and Protein Content of Extracted Starch: Nitrogen in starch powder was analyzed based on a combustion method (AOAC 992.23) using a nitrogen determinator (Leco CN928, MI, USA). Pre-weighed sample was transferred to the sealed purge chamber to degas after which it was then combusted in the furnace (>1100 °C). Nitrogen oxide species (NO_x) were converted to N₂ in the heated reduction tube filled with copper. Nitrogen was determined in the thermal conductivity cell. A nitrogen-to-protein conversion factor of 6.25 was used to calculate protein content.

Interfacial Tension and Contact Angle: The interfacial tension was measured using a tensiometer (ramé-hart model 500, NJ, USA) with a 22gauge blunt-tip needle. Analysis of droplet images was performed using DROPimage advanced software (ramé-hart, NJ, USA) to assess the pendant shape. The interfacial tension between the 0.5 w/v % starch suspension and heptane was calculated utilizing the Young-Laplace equation.

To evaluate the contact angle, starch was cast into a flat pellet using a hydraulic press (250 bar, Mestra, Bizkaia, Spain). Water was dispensed onto the material surface and the contact angle was analyzed using a goniometer (ramé-hart model 500, NJ, USA).

Fabrication of Starch Hollow Particles: Amaranth starch extracted by 0.15 w/v% NaOH was used as a Pickering stabilizer to emulsify oil, forming an O/W emulsion. Heptane (b.p. 98 °C) was selected as the organic phase for the ease of removal. The oil fraction was 30 or 50 w/w%. The starch-to-oil ratio was 1:10 or 1:5. To prepare emulsions, the starch powder was dispersed in water, and heptane was added. The mixture was sheared at 16 000, 20 000, and 24 000 rpm for 1 min using a high-shear homogenizer (T25 digital Ultra-Turrax, 18-mm dispensing probe, IKA, NC, USA). The prepared emulsions were then incubated in a water bath (75 °C) and the temperature of the emulsion was monitored. When the temperature of the incubated emulsion reached 70 °C, it was immersed in an ice bath. The cooled emulsion (60 g) was transferred, dropwise, to absolute ethanol (240 mL at 20 °C). The suspension in ethanol was centrifuged at 20 g for 5 min, the pellet was collected and was washed with additional absolute ethanol and centrifuged two more times to remove water. To remove the organic phase, the ethanol-purified particles were washed with hexane and centrifuged at 20 g for 5 min, the pellet was collected, and any remaining solvent was evaporated in a vacuum desiccator (4.4 psi) overnight.

Starch Adsorption at Emulsion Droplet Surface: Emulsions were transferred to a separatory funnel. Due to the density contrast, emulsion droplets (heptane density = 0.684 g mL^{-1}) creamed, whereas free starch particles (starch density $\approx 1.5 \text{ g mL}^{-1}$) settled to the bottom within 48 h. The sedimented layer was collected and freeze-dried. The starch adsorption to the oil-water interface was evaluated as the ratio of free starch to the total starch content used for emulsification.

Examination of Microstructure: Pickering emulsions were examined using a Leica Model DMIL LED Inverted Phase Contrast Microscope. The droplet size of the emulsion droplets was analyzed by ImageJ software (v1.51, National Institute of Health) on > 300 droplets per sample. The dried starch and hollow starch colloidosomes were examined using scanning electron microscopy (SEM) (Zeiss Gemini 500, Germany). Dry samples were coated with Au-Pd using a sputter coater (Denton Desk V, NJ, USA) for 40 s at 30 mA and 2×10^{-4} m bar. Coated objects were scanned with 1 keV and imaged by a high-efficiency secondary electron detector with a 20.0 µm aperture.

Mercury Porosimetry: The porosity, bulk density, and pore size distribution of colloidosomes based on starch were evaluated using a mercury porosimeter (Autopore IV 9500, Micromeritics, AZ). Mercury, as a nonwetting liquid, was used with a surface tension (σ) of 485 mN m⁻¹ and a contact angle (θ) of 130°. The intrusion of mercury was performed from 0.3 to 30 000 psi. Pore equivalent capillary diameters (d) are calculated based on the Washburn equation: $d = \frac{-4\sigma cos\theta}{P}$, where P is the applied

X-Ray Diffractometry (XRD): The XRD patterns of the starch powder were analyzed using a Bruker D8 Advance ECO powder diffractometer (MA, USA) at 40 kV and 25 mA with Cu K α radiation. The starch powder was scanned from 5° to 40°. The scanning step size was 0.02° with 0.8 s per step.

Attenuated Total Reflectance-Fourier Transform Infrared Spectroscopy (FTIR): Starch samples were analyzed using an ATR-FTIR (Affinity-1S, Shimadzu). Samples were characterized from 400 to 4000 cm⁻¹ in transmittance mode with 4 cm⁻¹ resolution and 64 scans.

Solid-State Nuclear Magnetic Resonance (NMR): Solid-state crosspolarization magic angle spinning ¹³C nuclear magnetic resonance (¹³C CP/MAS NMR) data were acquired using a DSX-500 Bruker (11.7 T) system operating at 125.8 MHz. The measurements were conducted with a 4 mm Bruker MAS NMR probe. Spinal ¹H-decoupling was applied during signal acquisition. The sample was run at a spinning rate of 10 kHz, with a cross-polarization contact time of 0.5 ms, and a recycle delay of 2 s.

Rheological Measurements: The viscosity was conducted using a slurry with a rheometer (Anton Paar MCR501, Graz, Austria). A 25 mm parallel plate was used with the gap set at 0.5 mm. Measurement of 13 w/w%

ADVANCED FUNCTIONAL MATERIALS 16163028, 0, Downloaded from https://onlinelibrary.wiley.com/doi/10.1002/adfm.202313025 by Cornell University Library, Wiley Online Library on [11/042024]. See the Terms and Conditions (https://onlinelibrary.wiley

and-conditions) on Wiley Online Library for rules of use; OA articles are governed by the applicable Creative Commons

starch slurries was carried out at 20 °C. The shear stress (τ) and shear rate $(\dot{\gamma})$ were used to fit a Herschel-Bulkley model: $\tau=\tau_0+\kappa\dot{\gamma}^n$. Where κ is the consistency factor, τ_0 is the yield stress, and n is the flow index. To test the stability against mechanical stress, the secondary shear ramp was carried out after 30 s resting and the viscosity retention was evaluated.

Statistical Analysis: The statistical significance of the differences was determined using one-way analysis of variance (ANOVA) and Tukey's multiple comparison test in JMP Pro (Version 17, SAS Institute, USA) with a significance level set at p < 0.05. For non-normal distributions, the non-parametric Wilcoxon method was used for comparison.

Supporting Information

Supporting Information is available from the Wiley Online Library or from the author.

Acknowledgements

Funding for this project was provided by Tate & Lyle Solutions USA LLC. The authors would like to thank Weichang Liu from Tate & Lyle Solutions USA LLC for many fruitful and thoughtful discussions SVP Veronica Cueva also from Tate & Lyle Solutions USA LLC for supporting the funding of this work and Sara Vinarov for legal guidance. The authors also thank Kelley J. Donaghy for editing this manuscript. Cornell Center for Materials Research Shared Facilities, supported through the NSF MRSEC program (DMR-1719875), provided partial imaging data. The rheological and porosimetry characterizations were performed with the assistance of the Cornell Energy Systems Institute.

Conflict of Interest

The authors declare no conflict of interest.

Data Availability Statement

The data that support the findings of this study are available from the corresponding author upon reasonable request.

Keywords

colloidosomes, Pickering emulsion, porosity, rheology, starch

Received: October 20, 2023 Revised: February 23, 2024 Published online:

- [1] A. Einstein, Ann. Phys. 1905, 17, 208.
- [2] J. Mewis, N. J. Wagner, Colloidal Suspension Rheology, 1st ed., Cambridge University Press, NY, 2012.
- [3] G. K. Batchelor, J Fluid Mech 1977, 83, 97.
- [4] J. J. Stickel, R. L. Powell, Annu. Rev. Fluid Mech. 2005, 37, 129.
- [5] S. Assenza, R. Mezzenga, Nat Rev Phys 2019, 1, 551.
- [6] R. Mezzenga, P. Schurtenberger, A. Burbidge, M. Michel, Nature Mater 2005, 4, 729.
- [7] J. Shintake, V. Cacucciolo, D. Floreano, H. Shea, Adv. Mater. 2018, 30, 1707035.
- [8] M. Huang, J. Wang, C. Tan, Food Hydrocolloids 2021, 118, 106742.
- [9] S.-E. Phan, W. B. Russel, J. Zhu, P. M. Chaikin, J. Chem. Phys. 1998, 108, 9789.

- [10] D.-H. Nguyen, E. Azéma, P. Sornay, F. Radjai, Phys Rev E 2015, 91, 032203.
- [11] E. Azéma, S. Linero, N. Estrada, A. Lizcano, Phys Rev E 2017, 96, 022902.
- [12] P. Ruckdeschel, A. Philipp, M. Retsch, Adv. Funct. Mater. 2017, 27, 1702256.
- [13] B. Lu, E. Hu, R. Xie, K. Yu, F. Lu, R. Bao, C. Wang, G. Lan, F. Dai, Bioact Mater 2022, 16, 372.
- [14] C. Tan, M. Arshadi, M. C. Lee, M. Godec, M. Azizi, B. Yan, H. Eskandarloo, T. W. Deisenroth, R. H. Darji, T. V. Pho, A. Abbaspourrad, ACS Nano 2019, 13, 9016.
- [15] H. Wu, X. Du, X. Meng, D. Qiu, Y. Qiao, Nat. Commun. 2021, 12, 6113.
- [16] C. Hoyle, S. Dai, R. Tanner, A. Jabbarzadeh, J. Non-Newtonian Fluid Mech. 2020, 276, 104235.
- [17] C. Wang, J. Yan, X. Cui, D. Cong, H. Wang, Colloids Surf. A 2010, 363, 71.
- [18] W. Wang, D. Li, S. Li, H. Zeng, J. Zhang, J. Environ. Chem. Eng. 2022, 10. 107230.
- [19] J. Guo, L. Kong, B. Du, B. Xu, Int. J. Biol. Macromol. 2019, 130, 357.
- [20] J. N. BeMiller, K. C. Huber, Annu. Rev. Food Sci. Technol. 2015, 6, 19.
- [21] Z. Xue, P. Wang, A. Peng, T. Wang, Adv. Mater. 2019, 31, 1801441.
- [22] A. D. Dinsmore, M. F. Hsu, M. G. Nikolaides, M. Marquez, A. R. Bausch, D. A. Weitz, *Science* 2002, 298, 1006.
- [23] M. R. Bailey, F. Grillo, N. D. Spencer, L. Isa, Adv. Funct. Mater. 2022, 32. 2109175.
- [24] M. Wei, Y. Lin, Y. Qiao, Giant 2023, 13, 100143.
- [25] K. L. Thompson, M. Williams, S. P. Armes, J. Colloid Interface Sci. 2015, 447, 217.
- [26] J. Wu, G.-H. Ma, Small 2016, 12, 4633.
- [27] F. Zhu, Trends Food Sci. Technol. 2019, 85, 129.
- [28] P. Li, A. Kierulf, J. Wang, M. Yaghoobi, J. Whaley, J. Smoot, M. P. Herrera, A. Abbaspourrad, ACS Appl. Mater. Interfaces 2022, 14, 24055.
- [29] A. Kierulf, I. Mosleh, J. Li, P. Li, A. Zarei, L. Khazdooz, J. Smoot, A. Abbaspourrad, Sci. Adv. 2024, 10, eadi7069.
- [30] M. Majzoobi, A. Farahnaky, Food Hydrocolloids 2021, 111, 106393.
- [31] P. Li, A. Kierulf, A. Abbaspourrad, Food Hydrocolloids 2021, 112, 106311.
- [32] J. L. Slavin, Adv Nutr 2013, 4, 351S.
- [33] D. Mozaffarian, Nutr Rev 2017, 75, 19.
- [34] A. Dumoitier, V. Abbo, Z. T. Neuhofer, B. R. McFadden, Obesity Science & Practice 2019, 5, 581.
- [35] R. Schoenlechner, S. Siebenhandl, E. Berghofer, In Gluten-Free Cereal Products and Beverages (Eds.: E. K. Arendt, F. Dal Bello), Academic Press, San Diego, 2008, pp. 149–VI.
- [36] H. Choi, W. Kim, M. Shin, Starch Stärke 2004, 56, 469.
- [37] A. Kierulf, M. Enayati, M. Yaghoobi, J. Whaley, J. Smoot, M. P. Herrera, A. Abbaspourrad, ACS Appl. Mater. Interfaces 2022, 14, 57371.
- [38] M. Rayner, D. Marku, M. Eriksson, M. Sjöö, P. Dejmek, M. Wahlgren, Colloids Surf. A 2014, 458, 48.
- [39] M. Sjöö, S. C. Emek, T. Hall, M. Rayner, M. Wahlgren, J. Colloid Interface Sci. 2015, 450, 182.
- [40] T. F. Tadros, Emulsion Form. Stab. 2013, 1.
- [41] A. F. Doblado-Maldonado, F. Janssen, S. V. Gomand, B. De Ketelaere, B. Goderis, J. A. Delcour, Food Hydrocolloids 2017, 63, 265.
- [42] S. J. McGrane, D. E. Mainwaring, H. J. Cornell, C. J. Rix, Starch Stärke 2004, 56, 122.
- [43] F. Porcheron, P. A. Monson, M. Thommes, Langmuir 2004, 20, 6482.
- [44] R. N. Waduge, S. Xu, K. Seetharaman, Carbohydr. Polym. 2010, 82, 786



www.advancedsciencenews.com



www.afm-journal.de

16163028, 0, Downloaded from https://onlinelibrary.wiley.com/doi/10.1002/adfm.202313025 by Cornell University Library, Wiley Online Library on [11/04/2024]. See the Terms

and-conditions) on Wiley Online Library for rules of use; OA articles are governed by the applicable Creative Commons I

- [45] J. A. Boxall, C. A. Koh, E. D. Sloan, A. K. Sum, D. T. Wu, Langmuir 2012, 28, 104.
- [46] T.-J. Lim, B. Smith, D. L. McDowell, Acta Mater. 2002, 50, 2867.
- [47] H. Wang, X. Zhu, L. Tsarkova, A. Pich, M. Möller, ACS Nano 2011, 5, 3937.
- [48] P. Olsson, S. Teitel, Phys. Rev. Lett. 2012, 109, 108001.
- [49] Z. Lv, K. Yu, S. Jin, W. Ke, C. Fei, P. Cui, G. Lu, Starch Stärke 2019, 71, 1800175.
- [50] S. Sridharan, M. B. J. Meinders, J. H. Bitter, C. V. Nikiforidis, *Langmuir* 2020, 36, 12221.
- [51] M. N. Lee, H. K. Chan, A. Mohraz, *Langmuir* **2012**, *28*, 3085.
- [52] D. J. French, P. Taylor, J. Fowler, P. S. Clegg, J. Colloid Interface Sci. 2015, 441, 30.
- [53] H. Schubert, K. Ax, O. Behrend, Trends Food Sci. Technol. 2003, 14, 9.
- [54] B. Lauke, Compos. Sci. Technol. 2008, 68, 3365.